*Inorg. Chem.* **2008**, *47*, 11048−11056

# Magnetic Properties and Negative Colossal Magnetoresistance of the Rare Earth Zintl phase $EuIn_2As_2$

**Andrea M. Goforth,[†] Peter Klavins,[‡] James C. Fettinger,[†] and Susan M. Kauzlarich*,[†]**

*Department of Chemistry and Department of Physics, University of California, One Shields Avenue, Davis, California 95616*

Received July 9, 2008

Large, high quality single crystals of a new Zintl phase, $EuIn_2As_2$, have been synthesized from a reactive indium flux. $EuIn_2As_2$ is isostructural to the recently reported phase $EuIn_2P_2$, and it is only the second reported member of the group of compounds with formula $AM_2X_2$ (A = alkali, alkaline earth, or rare earth cation; M = transition or post-transition metal; and X = Group 14 or 15 element) that crystallizes in the hexagonal space group $P6_3/mmc$ ($a$ = 4.2067(3) Å, $c$ = 17.889(2) Å and $Z$ = 2). The structure type contains layers of $A^{2+}$ cations separated by $[M_2X_2]^{2-}$ layers along the crystallographic $c$-axis. Crystals of the title compound were mounted for magnetic measurements, with the crystallographic $c$-axis oriented either parallel or perpendicular to the direction of the applied field. The collective magnetization versus temperature and field data indicate two magnetic exchange interactions near 16 K, one involving $Eu^{2+}\cdots Eu^{2+}$ intralayer coupling and the other involving $Eu^{2+}\cdots Eu^{2+}$ coupling between layers. $EuIn_2As_2$ is metallic and magnetoresistive, as is the isostructural phosphide, and both compounds have coincident resistivity and magnetic ordering transitions, consistent with the observation of colossal magnetoresistance. Negative colossal magnetoresistance (MR = $\{[\rho(H) - \rho(0)]/\rho(H)\} \times 100\%$) of up to −143% (at $T$ = 17.5 K, $H$ = 5 T) is observed for $EuIn_2As_2$, approximately half of that observed for the more resistive phosphide, which has a higher magnetic ordering temperature and local moment coupling strength.

## Introduction

Since the first presentation of the Zintl concept in the early 1900s by Eduard Zintl, Zintl phases have received great interest because of their fascinating structural variety and because of their useful synthetic and materials applications.[1] Zintl phases are defined as valence precise compounds of the heavier main group elements where there is complete charge transfer from a highly electropositive element (or elements), generally from Group 1 or 2, to a more electronegative main group element (or elements), generally from Groups 13−15. The unique structural features of traditional Zintl phases, that is, their closed shell electron configurations, frequently catenated nature, structural complexity, and topological variety, as well as their heavy element compositions, lead to their useful materials properties.

Zintl phases with extended, multidimensional anion structures are by definition semiconductors or semimetals because they obey the octet rule; consequently, activated electronic properties and electronic band gaps are expected for these compounds.[2] However, because they are generally composed of heavy elements, the band gap is usually very small; thus, Zintl phases have been studied for unusual opto-electronic properties,[3] as well as for thermoelectric applications,[4−6] in which the structural complexity and low electrical resistivity contribute to high values for the thermoelectric figure of merit, zT (zT = $S^2T/\rho\kappa$, $S$ = Seebeck coefficient, $T$ = temperature, $\rho$ = electrical resistivity, $\kappa$ = thermal conductivity).

* To whom correspondence should be addressed. E-mail: smkauzlarich@ucdavis.edu.
† Department of Chemistry.
‡ Department of Physics.

(1) Kauzlarich, S. M. *Chemistry, Structure and Bonding of Zintl Phases and Ions: Selected Topics and Recent Advances*; VCH Publishers., Inc.: New York, 1996; p 306.
(2) Kauzlarich, S. M.; Chan, J. Y.; Taylor, B. R. Exploitation of Zintl Phases in the Pursuit of Novel Magnetic and Electronic Materials. In *Inorganic Materials Synthesis*; Winter, C. H., Hoffman, D. M., Eds.; American Chemical Society: Washington, D.C., 1999; pp 15−27.
(3) Burch, K. S.; Schafgans, A.; Butch, N. P.; Sayles, T. A.; Maple, M. B.; Sales, B. C.; Mandrus, D.; Basov, D. N. *Phys. Rev. Lett.* **2005**, *95*, 046401-1.
(4) Kauzlarich, S. M.; Brown, S. R.; Snyder, G. J. *Dalton Trans.* **2007**, *21*, 2099.
(5) Brown, S. R.; Kauzlarich, S. M.; Gascoin, F.; Snyder, G. J. *Chem. Mater.* **2006**, *18*, 1873.
(6) Kanatzidis, M. G. *Chem. Mater.* **1999**, *11*, 3154.



10.1021/ic801290u CCC: $40.75 
Published on Web 10/29/2008

Rather than alkali or alkaline earth cations, rare earth cations may also serve as the electropositive species in Zintl compounds to achieve the same complexity and variety, and introduction of magnetic ions additionally results in a new set of properties achievable in Zintl phases. Specifically, interactions between localized spins of magnetic rare earth cations and delocalized spins of mobile carriers result in interesting electro-magnetic phenomena, such as magnetoresistance (MR), which involves changes in the electrical resistivity of a material with changes in the magnitude of the applied magnetic field (H). Our previous studies on the transport properties of a family of alkaline earth and rare earth-containing magnetic Zintl phases having the $Ca_{14}AlSb_{11}$ structure type, that is, $A_{14}MPn_{11}$ (A = Sr, Ca, Ba, Yb, Eu; M = In, Mn; Pn = P, As, Sb, Bi),[7] have indicated an intimate correlation between the onset of magnetic ordering events and changes in electrical resistivity, a feature which is typical of colossal magnetoresistant (CMR) materials, such as $Eu_xCa_{1-x}B_6$[8−10] and the perovskite manganites.[11−13] Furthermore, CMR is generally associated with materials having a Fermi energy lying near a metal−insulator border, and the $A_{14}MPn_{11}$ family of magnetoresistive materials range in their electrical behavior from semiconducting to metallic,[7] dependent upon their composition, for example, $Sr_{14}MnAs_{11}$ is a semiconductor and $Sr_{14}MnBi_{11}$ is metallic. Interestingly in the $A_{14}MPn_{11}$ compounds, the magnetically ordering cations are separated by a distance too large for direct coupling or superexchange, and the observation of both magnetic ordering and magnetoresistance is postulated to occur via a double exchange mechanism,[1,14−16] such as Rudderman−Kittel−Kasuya−Yosida (RKKY) coupling, where the local spins are communicated via delocalized carrier wave functions.

We have more recently observed large negative CMR (−298% at $T = 24$ K, $H = 5$ T) in a Zintl phase having a new structure type: $EuIn_2P_2$, which crystallizes in the hexagonal space group $P6_3/mmc$, and has $[In_2P_2]^{2-}$ layers separated by layers of $Eu^{2+}$ cations along the crystallographic *c*-axis.[17] Coincident magnetic ordering and resistivity transitions are observed for this compound; as are two $Eu^{2+}\cdots Eu^{2+}$ magnetic exchange interactions, where the magnetic coupling also likely occurs via indirect exchange, as evidenced by large Eu···Eu distances between magnetically coupled layers. The temperature dependence of the resistivity indicated that the phase was metallic, with an increase in the zero field resistivity just above the magnetic ordering temperature, followed by a sharp decrease in the resistivity in the temperature-induced, magnetically ordered state. The resistivity increase is suppressed with increasing magnetic field, indicating that the magnetic field-enhanced alignment of the local cation spins decreases the spin scatter of the delocalized carriers, resulting in decreased resistivity with increasing magnetic field, analogously to other reported CMR materials. Additionally, recent magneto-optical results show enhancement effects for $EuIn_2P_2$ similar to those reported for the CMR compound $EuB_6$.[18,19]

In light of our current program aimed at the synthesis and structural characterization of new, small band gap materials for thermoelectric applications, and because of the observation of colossal magnetoresistance in the europium-containing magnetic Zintl phases we have characterized to date, we have set out to draw correlations between material composition and structure and the observed magnetic/magneto-electronic properties. Additionally, superconductivity has been observed for other $AM_2X_2$ compounds,[20] as well as for other magnetically ordering magnetoresistive compounds,[21] further motivating our synthetic and charge transport studies. Herein, we present the anisotropic magnetic properties and magnetoresistive properties of a new Zintl compound, $EuIn_2As_2$, which is isostructural to $EuIn_2P_2$ but contains a heavier pnicogen element. By synthesizing families of Zintl phases having the same stoichiometry but differing compositions or structure types, we can deduce trends in the effects of element composition and crystal structure on the observed material properties, for example, the extent of magnetoresistance.

## Experimental Section

**Materials.** All reagents were handled under an inert atmosphere, either $N_2$ or Ar. Eu ribbon (3 mm, 99.999%, Ames Laboratory) was first brushed to remove the oxidized layer and then cut into small pieces. Crushed elemental As (polycrystalline lump, 99.9999+% puratronic, J. Matthey), and elemental In (3 mm teardrops, 99.99%, Cerac) were used as received.

**Synthesis - General Considerations.** For each reaction, the elements were loaded into a 5 mL alumina crucible in the following order: flux, elements, flux, where the Group 13 metal in large excess serves as the flux. The crucible, sandwiched between two layers of tightly packed quartz wool, was subsequently sealed under ~1/5 atm Ar in a fused silica ampule. The reaction vessel was then heated in a box furnace in an upright position, using various temperature schemes and stoichiometric ratios, as described below. At the end of the temperature scheme, the hot ampule was removed from the furnace, inverted, and centrifuged to remove the molten, reactive flux.

(7) Kauzlarich, S. M.; Payne, A. C.; Webb, D. J. Magnetism and Magnetotransport Properties of Transition Metal Zintl Isotypes. In *Magnetism: Molecules to Materials III*; Miller, J. S., Drillon, M., Eds.; Wiley-VCH: Weinheim, 2002; pp 37−62.
(8) Wigger, G. A.; Monnier, R.; Ott, H. R.; Young, D. P.; Fisk, Z. *Phys. Rev. B* **2004**, *69*, 1251181.
(9) Wigger, G. A.; Beeli, C.; Felder, E.; Ott, H. R.; Bianchi, A.; Fisk, Z. *Phys. Rev. Lett.* **2004**, *93*, 147203-1.
(10) Brooks, M. L.; Lancaster, T.; Blundell, S. J.; Pratt, F. L.; Pham, L. D.; Fisk, Z., *Physica B* **2006**, *374−375*, 26.
(11) Jin, S.; Tiefel, T. H.; McCormack, M.; Fastnacht, R. A.; Ramesh, R.; Chen, L.-H. *Science* **1994**, *264*, 413.
(12) Jin, S.; McCormack, M.; Tiefel, T. H.; Ramesh, R. *J. Appl. Phys.* **1994**, *76*, 6929.
(13) Ramirez, A. P. *J. Appl. Phys.* **1997**, *9*, 8171.
(14) Rehr, A.; Kuromoto, T. Y.; Kauzlarich, S. M.; Del Castillo, J.; Webb, D. J. *Chem. Mater.* **1994**, *6*, 93.
(15) Chan, J. Y.; Wang, M. E.; Rehr, A.; Webb, D. J.; Kauzlarich, S. M. *Chem. Mater.* **1997**, *9*, 2132.
(16) Chan, J. Y.; Olmstead, M. M.; Kauzlarich, S. M.; Webb, D. J. *Chem. Mater.* **1998**, *10*, 3583.
(17) Jiang, J.; Kauzlarich, S. M. *Chem. Mater.* **2006**, *18*, 435.
(18) Pfuner, F.; Degiorgi, L.; Ott, H.-R.; Bianchi, A.; Fisk, Z. *Phys. Rev. B* **2008**, *77*, 024417-1.
(19) Broderick, S.; Ruzicka, B.; Degiorgi, L.; Ott, H. R.; Sarrao, J. L.; Fisk, Z. *Phys. Rev. B* **2002**, *65*, 121102-1.
(20) Braun, H. F.; Engel, N.; Parthé, E. *Phys. Rev. B* **1983**, *28*, 1389.
(21) Tróc, R. *J. Alloys Compd.* **2006**, *423*, 21.

**Synthesis of $EuIn_2As_2$.** Large single crystals of $EuIn_2As_2$ were synthesized directly from the elements in a reactive indium flux using a 3:36:9 (Eu/In/As) molar ratio (10 g total weight, 79 wt % In, 75 at. % In). The mixture was heated at the rate of 60 °C/hr to 1100 °C and maintained at this temperature for 12 h before it was slow-cooled to 700 °C at a rate of 2 °C/hr. The ampule was removed from the furnace at 700 °C, inverted, and centrifuged to remove the molten indium flux. The reaction vessel was broken in air to yield large, black hexagonal plate crystals of $EuIn_2As_2$ in addition to lesser quantities of large, silver block crystals of $Eu_3In_2As_4$ (isostructural to $Eu_3In_2P_4$)[22] and large black, block crystals of $Eu_3InAs_3$ (isostructural to $Eu_3InP_3$),[23] which were initially identified by powder X-ray diffraction (XRD) and subsequently by single crystal XRD. The phase and distribution of the reaction products can be adjusted primarily by adjusting the starting flux composition, with more concentrated solutions and a stoichiometric excess of As leading to greater quantities of the desired phase, $EuIn_2As_2$. Further optimization of the flux synthesis conditions should result in a phase pure material, and important parameters for optimizing Zintl and intermetallic molten metal flux reactions have been reviewed in the literature.[24,25] However, since our synthetic objective was to obtain large single crystals of this phase for oriented magnetic and charge transport measurements, the reaction conditions were not further optimized to obtain a phase pure sample. Finally, if large quantities of phase pure samples are desired, it is likely that they can be obtained from neat, stoichiometric reactions of the elements, although this method would result in polycrystalline materials not suitable for the property measurements reported herein.

**Crystal Structure Determinations.** X-ray intensity data were collected on a suitable single crystal of $EuIn_2As_2$ at 90(2) K using a Bruker SMART 1000 CCD-based diffractometer (Mo Kα radiation, $\lambda = 0.71073$ Å).[26] Raw data frame integration and Lorentz and polarization corrections were performed using the SAINT+ program.[26] The data were corrected for absorption effects based on fitting a function to the empirical transmission surface, as sampled by multiple equivalent reflections with the program SADABS.[26] Direct methods structure solution and full-matrix least-squares refinement against $F^2$ were performed with SHELXTL.[27] X-ray data collection and structure refinement details for $EuIn_2As_2$ are listed in Table 1. Selected bond distances and angles are listed in Table 2.

**Powder X-ray Diffraction.** Representative samples from each reaction performed were ground to fine powders in air using an agate mortar and pestle. Powder diffraction patterns were collected in air on an INEL diffractometer (Co Kα radiation, $\lambda = 1.78890$ Å) and compared with diffraction patterns calculated from single crystal data using the program CrystalDiffract.[28] Powder XRD was used to qualitatively identify the phases present upon completion of each flux reaction.

**Magnetic Measurements.** Magnetic measurements were recorded on oriented single crystals using a Quantum Design MPMS superconducting quantum interference device (SQUID).

For $EuIn_2As_2$, the *a* and *c*-axis orientations of large crystals (having hexagonal, platelike habits, weighing between 0.44 and 3.26 mg) were determined by single crystal X-ray diffraction prior to measurement; and the thin dimension of the plates was determined to coincide with the crystallographic *c*-axis. The crystals were fixed in the desired orientations on either thin Mylar strips or the end of a straw covered with Kapton tape. The samples were then covered with Kapton tape and mounted symmetrically in drinking straws, which were used as the sample holders. This method of sample measurement provides negligible background contribution from the sample holder, and consequently, the data were not corrected. Magnetic susceptibility as a function of temperature (zero field-cooled (ZFC)/field-cooled (FC) sequences, 2−320/280−2 K) was subsequently measured with either the *c*-axis parallel to the applied field (*a*-*b* plane perpendicular) or the *c*-axis perpendicular to the applied field (*a*-*b* plane parallel) at field strengths of 1, 0.1, and 0.01 T. Inverse susceptibility as a function of temperature was fit to the Curie−Weiss law, $\chi^{-1} = T/C - \theta/C$, to determine the effective magnetic moment of europium. However, to minimize the effects of any short-range magnetic ordering of the spins above the transition temperature, only the data collected above 50 K were fit. Magnetization as a function of field strength was also measured between −4 and 4 T for both orientations at $T = 5$ K.

**Charge Transport Properties.** Four platinum leads were attached with silver paint to a clean (001) face of a hexagonal plate crystal of $EuIn_2As_2$ for transport measurements. The pertinent dimensions of the leads and crystal area were: 0.30 × 0.66 × 0.12 $mm^3$ (length × width × height), where length is the distance between the innermost silver paint contacts of the voltage leads, width is approximated as the distance across the *a*-*b* plane coincident with the voltage leads, and height is the thin plate dimension. Corresponding measurements in the perpendicular orientation were not performed because of the thin, platelike nature of the crystals and the difficulty of attaching leads. A Keithley model 224 current source and model 181 voltmeter were interfaced to the SQUID magnetometer for the measurement. A constant current (*I*) of 1 mA was applied across the crystal in the *a*-*b* plane

**Table 1.** Crystal Data and Structure Refinement for $EuIn_2As_2$

| | |
|---|---|
| empirical formula | $EuIn_2As_2$ |
| formula weight (g/mol) | 531.44 |
| temperature (K) | 90(2) |
| wavelength (Å) | 0.71073 |
| space group | *P*6(3)/*mmc* (No. 194) |
| lattice parameters (Å, deg) | $a = 4.2067(3)$ |
| | $b = 4.2067(3)$ |
| | $c = 17.889(2)$ |
| volume ($Å^3$) | 274.16(4) |
| *Z* | 2 |
| density (calculated, $Mg/m^3$) | 6.438 |
| absorption coefficient ($mm^{-1}$) | 31.442 |
| theta range (deg) | 2.28 to 27.47 |
| reflections collected | 2314 |
| independent reflections | 158 |
| data/restraints/parameters | 158/0/10 |
| goodness-of-fit on $F^2$ | 1.175 |
| final *R* indices $[I > 2\sigma(I)]^a$ | R1 = 0.0101 |
| | wR2 = 0.0218 |
| *R* indices (all data) | R1 = 0.0165 |
| | wR2 = 0.0234 |
| extinction coefficient | 0.0031(3) |
| largest diff. peak and hole ($e \cdot Å^{-3}$) | 0.457 and −0.592 |

[a] $R1 = [\sum||F_o| - |F_c||]/\sum|F_o|$; $wR2 = \{[\sum w[(F_o)^2 - (F_c)^2]^2]\}^{1/2}$; $w^{-1} = [\sigma^2(F_o) + (0.0471P)^2 + (0.5945P)]$ where $P = [\max(F_o^2,0) + 2F_c^2/3]$.

**Table 2.** Selected Inter-Atomic Distances (Å) and Angles (deg) for $EuIn_2As_2$

| | | | |
|---|---|---|---|
| In−In | 2.765(1) | In−As | 2.6946(4) |
| Eu−As | 3.0976(4) | | |
| As−In−In | 115.67(2) | As−In−As | 102.63(2) |
| As−Eu−As (*cis*) | 85.54(1) and 94.46(1) | As−Eu−As (*trans*) | 180.0 |


(22) Jiang, J.; Olmstead, M. M.; Kauzlarich, S. M.; Lee, H.-O.; Klavins, P.; Fisk, Z. *Inorg. Chem.* **2005**, *44*, 5322.
(23) Jiang, J.; Payne, A. C.; Olmstead, M. M.; Lee, H.-O.; Klavins, P.; Fisk, Z.; Kauzlarich, S. M. *Inorg. Chem.* **2005**, *44*, 2189.
(24) Kanatzidis, M. G.; Pottgen, R.; Jeitschko, W. *Angew. Chem., Int. Ed.* **2005**, *43*, 6996.
(25) Canfield, P. C.; Fisk, Z. *Philos. Mag. B* **1992**, *65*, 1117.
(26) *SMART, SAINT+, and SADABS*; Bruker AXS: Madison, WI, 1998.
(27) Sheldrick, G. M. *SHELXL-97*; Bruker AXS: Madison, WI, 1997.
(28) *CrystalDiffract*; CrystalMaker Software Limited: Oxfordshire, U.K., 2006.

through the two outer leads, and the voltage drop ($V$) was measured across the innermost leads. The measured voltage is proportional to the resistance ($R$) of the sample ($V = IR$), and the resistivity ($\rho$) was determined by taking into account the physical dimensions of the charge carrier path ($\rho = RA/l$, $A$ = cross-sectional area, $l$ = length). Resistivity as a function of temperature was measured at several applied fields, ranging from 0−5 T. Magnetoresistance was calculated as: MR = $\{[\rho(H) - \rho(0)]/\rho(H)\} \times 100\%$.

## Results and Discussion

**Crystal Structures and Diversity in the 122 Structure Type.** After the advent of CCD diffractometers for single crystal structure determination, the field of Zintl compounds has witnessed an enormous explosion, both in terms of the number of new members and the variety in structure type. In fact, even for ternary Zintl compounds having the same, relatively simple stoichiometry, variety in structure type is observed, and this structural diversity is exemplified by Zintl compounds of the composition $AM_2X_2$, where A is an electropositive (Group 1, Group 2, or rare earth) element, M is a transition or post-transition element, and X is an element from Group 14 or Group 15.

The two most frequently occurring structure types for compounds of the composition $AM_2X_2$ are the tetragonal $ThCr_2Si_2$ (*I*4/*mmm*) and trigonal $CaAl_2Si_2$ ($P\bar{3}m1$) structure types,[29−32] where $[M_2X_2]^{n-}$ anionic layers are separated by cations along some crystallographic direction. Additionally, $AM_2X_2$ compounds sometimes crystallize into structures having other 2-dimensional, covalently connected networks, for example $EuZn_2Ge_2$ with the layered $CaBe_2Ge_2$ (tetragonal, *P*4/*nmm*) structure type,[30] while 3-dimensional anionic networks, for example the $[Ga_2Sb_2]^{2-}$ covalent network of $BaGa_2Sb_2$,[33] are even less common. However, our group has recently reported the synthesis and structural characterization of a new, hexagonal $AM_2X_2$ structure type for a new Zintl compound, $EuIn_2P_2$, that also contains 2-dimensional covalently bonded networks (*P*6$_3$/*mmc*).[17] This hexagonal $AM_2X_2$ phase displays structural similarities to both the 2-dimensional layered phases $ThCr_2Si_2$ and $CaAl_2Si_2$, by having alternating layers of $[M_2X_2]^{n-}$ and cations, as well as to the 3-dimensional covalent network of the binary phase $CaIn_2$, by removal of one-half of the $A^{2+}$ cation layers and by breaking the In−In bonds between alternate layers interleaved by the remaining $A^{2+}$. The title compound, $EuIn_2As_2$, is isostructural to the hexagonal $EuIn_2P_2$ phase; its structure (Figure 1a), which obeys the octet rule and adheres to the Zintl formalism, is briefly described below.

$EuIn_2As_2$ contains $[In_2As_2]^{2-}$ layers, which are charge balanced by $Eu^{2+}$ cation layers, as evidenced by magnetic data (vide infra), and cation and anion layers alternate along the crystallographic *c*-axis in this structure type. Within the

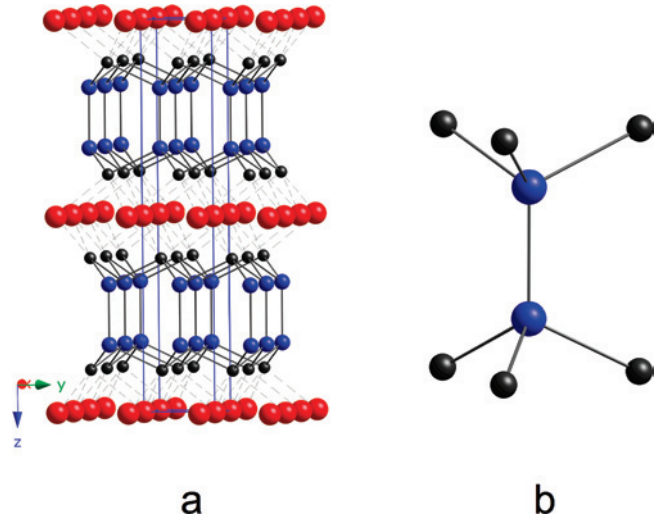


**Figure 1.** (a) (100) view of the crystal structure of $EuIn_2As_2$ and (b) view of a single $[In_2As_6]$ eclipsed dumbbell, the trigonal prismatic building unit of $[In_2As_2]^{2-}$ layers in $EuIn_2As_2$. Eu, In, and As atoms are shown as red, blue, and black spheres, respectively. Eu···As interactions are shown as dashed lines; covalent bonds, solid lines.

M−X layers, each As center is found in a pyramidal coordination environment, is bonded to three In centers, and has a lone pair. The In centers in the layers are found in 4-coordinate, tetrahedral environments and are each bonded to one In and three As atoms, resulting in the formation of $[In_2As_6]$ eclipsed, ethane-like dumbbells (Figure 1b). Each $[In_2As_6]$ dumbbell can be viewed as a trigonal prismatic building unit, which shares its three long edges ($[In_2As_{6/3}]$) with identical building units to form $In_3As_3$ six-membered rings when the structure is viewed along the *c*-axis of the hexagonal unit cell. A similar, six-membered ring arrangement exists in $CaAl_2Si_2$ when viewed along its *c*-axis. However, in this structure type, both the Al and the Si of the $[Al_2Si_2]^{2-}$ layers are found in four-coordinate bonding environments (tetrahedral or "umbrella"), where each $MX_4$ tetrahedron shares edges with three others to yield corrugated, two-atom thick anionic layers. The differences in the layer structures of these two compounds can be rationalized on the basis of the formal charges of the atoms that constitute them. $[Al_2Si_2]^{2-}$ contains 16 electrons per formula unit, with each four-bonded aluminum having a 1− formal charge and each four-bonded silicon having a zero formal charge for an overall layer charge of 2− per formula unit. $[In_2As_2]^{2-}$, however, has two additional electrons per formula unit, which are accommodated as a lone pair on As. Thus, each As center exhibits a pyramidal rather than a tetrahedral coordination environment and contributes zero formal charge. The layer charge of $EuIn_2As_2$ is thus the result of the formal charges of 1− on each of the tetrahedral In atoms of the $[In_2As_6]$ dumbbells. Both $CaAl_2Si_2$ and $EuIn_2As_2$ are valence precise compounds. However, simple oxidation state assignment works to rationalize the former compound stoichiometry but fails for the latter ($[Ca^{2+}(Al^{3+})_2(Si^{4-})_2]$ versus $[Eu^{2+}(In^{3+})_2(As^{3-})_2]$).

The In−In bond distance of 2.765(1) Å in $EuIn_2As_2$ is similar to that found in $EuIn_2P_2$ (2.761(1) Å) but much

(29) Hellmann, A.; Löhken, A.; Wurth, A.; Mewis, A. *Z. Naturforsch.* **2007**, *62b*, 155.
(30) Grytsiv, A.; Kaczorowski, D.; Leithe-Jasper, A.; Rogl, P.; Godart, C.; Potel, M.; Noël, H. *J. Solid State Chem.* **2002**, *163*, 37.
(31) Brock, S. L.; Greedan, J. E.; Kauzlarich, S. M. *J. Solid State Chem.* **1994**, *113*, 303.
(32) Bobev, S.; Merz, J.; Lima, A.; Firtsch, V.; Thompson, J. D.; Sarrao, J. L.; Gillessen, M.; Dronskowski, R. *Inorg. Chem.* **2006**, *45*, 4047.
(33) Kim, S.-J.; Kanatzidids, M. G. *Inorg. Chem.* **2001**, *40*, 3781.

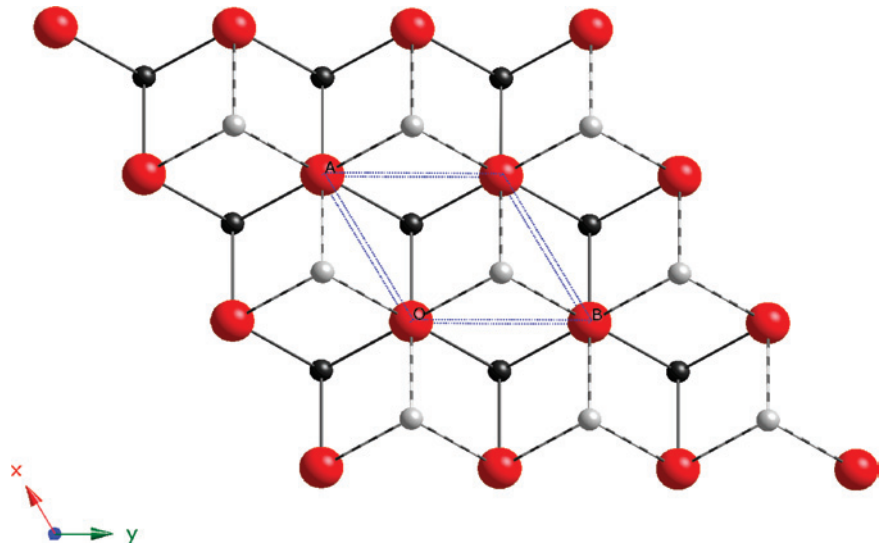


**Figure 2.** (001) view of a single layer of europium cations in $EuIn_2As_2$, highlighting the octahedral coordination sphere of As atoms from the anion layers above and below. Arsenic atoms belonging to different anion layers are distinguished by differing gray shades. Eu atoms are shown in red.

shorter than those in $CaIn_2$ ($3 \times 2.92$ Å, $1 \times 3.13$ Å),[34] which has a 3-dimensional homoatomic In network rather than a 2-dimensional heteroatomic In-Pn network. However, the pseudotetrahedral angles about the central $In_2$ dumbbells are similar in all three compounds: 102.63(2) and 115.67(2)° in $EuIn_2As_2$ (As−In−As and As−In−In, respectively, average = 109.15°), 102.58(4) and 115.70(3)° in $EuIn_2P_2$ (P−In−P and P−In−In, respectively, average = 109.14°), and 104.6 and 113.8° in $CaIn_2$ (In−In−In equatorial and In−In−In axial, respectively, average = 109.2°).[17,34] The In−As bond in the layer is 2.6946(4) Å, slightly longer than the sum of the covalent radii ($r_{In} + r_{As} = 2.61$ Å)[35] and within In−As covalent bond distances observed in other Zintl compounds having similar In local coordination environments.[36−38]

The local Eu coordination environment in $EuIn_2As_2$ is shown in Figure 2. The Eu atoms are coordinated in a distorted octahedral fashion (*cis* As−Eu−As angles are 85.54(1) and 94.46(1)°) to arsenic atoms from the anion layers above and below, at distances shorter than the sum of the associated covalent radii (Eu−As = 3.0976(4) Å in $EuIn_2As_2$, $r_{Eu} + r_{As} = 3.17$ Å);[35] although, because of the $f^7$ electronic configuration of $Eu^{2+}$, the bonding interaction between Eu atoms and the anionic layers is likely primarily ionic.[39] The $EuAs_6$ octahedra are connected to one another by sharing six edges with neighboring octahedra in the Eu−As layer. The shortest distance between $Eu^{2+}$ cations in the same layer is 4.207(3) Å, which is the same as the length of the hexagonal unit cell *a*- and *b*-axes. Additionally, the hexagonal space symmetry sets up an equilateral triangular arrangement of Eu cations with the same intra-atomic separation, which could lead to spin frustration in the intralayer magnetic exchange interaction. The shortest interlayer Eu···Eu distance of 8.945(2) Å is one-half of the crystallographic *c*-axis repeat distance.

**Magnetism.** Plots of molar susceptibility versus temperature for $EuIn_2As_2$ single crystals mounted in two different crystallographic orientations relative to the applied field (*H*) are shown in Figure 3. The inset of Figure 3a shows a plot of inverse molar susceptibility versus temperature for the 1 T measurement (ZFC), from which the molar Curie constant was determined to be 7.84(1) emu K/mol, corresponding to a spin-only magnetic moment of 7.90(1) $\mu_B$. This value agrees well with the spin-only moment of 7.94 $\mu_B$ calculated for an $f^7$ ion, and indicates a europium oxidation state of +2. A Weiss constant ($\theta$) of +17.40(2) K was also calculated using the same data set, and this value is close to the observed magnetic ordering temperature of 16 K (vide infra). The high temperature data ($\chi^{-1}$ vs *T*) collected in smaller fields ($H$ = 0.1, 0.01 T) was also fit to the Curie−Weiss law; as were replicate data sets collected at 1 T; and the values obtained from these fits are consistent with those reported above and with the theoretical spin only moment of $Eu^{2+}$.

At temperatures less than approximately 45 K, the temperature dependence of the susceptibility is anisotropic with respect to crystallographic orientation as indicated by the divergence of the curves, while above this temperature the susceptibility is isotropic (see Supporting Information, Figure S1). For all field strengths, the susceptibility in the anisotropic temperature regime is largest when the *c*-axis is oriented perpendicular to the applied magnetic field, indicating that the easy magnetization direction for ferromagnetic coupling is in the *a*-*b* plane. Below 45 K, the susceptibility rises rapidly with decreased temperature, particularly in the perpendicular orientation, indicating a ferromagnetic exchange interaction. However, in the low field data sets ($H$ = 0.1, 0.01 T, Figures 3b and 3c, respectively), an obvious downturn in the susceptibility is observed for both orientations at around $T_N = 16$ K ($T_N = 14$ K in the 1 T data set, *c*-axis parallel to *H*), indicative of antiferromagnetic ordering

(34) Nuspl, G.; Polborn, K.; Evers, J.; Landrum, G. A.; Hoffmann, R. *Inorg. Chem.* **1996**, *35*, 6922.
(35) Cordero, B.; Gómez, V.; Platero-Prats, A. E.; Revés, M.; Echeverria, J.; Cremades, E.; Barragán, F.; Alvarez, S. *Dalton Trans.* **2008**, 2832.
(36) Gascoin, F.; Sevov, S. C. *Inorg. Chem.* **2001**, *40*, 6254.
(37) Gascoin, F.; Sevov, S. C. *Inorg. Chem.* **2002**, *41*, 2292.
(38) Gascoin, F.; Sevov, S. C. *Inorg. Chem.* **2003**, *42*, 8567.
(39) Pöttgen, R.; Johrendt, D. *Chem. Mater.* **2000**, *12*, 875.

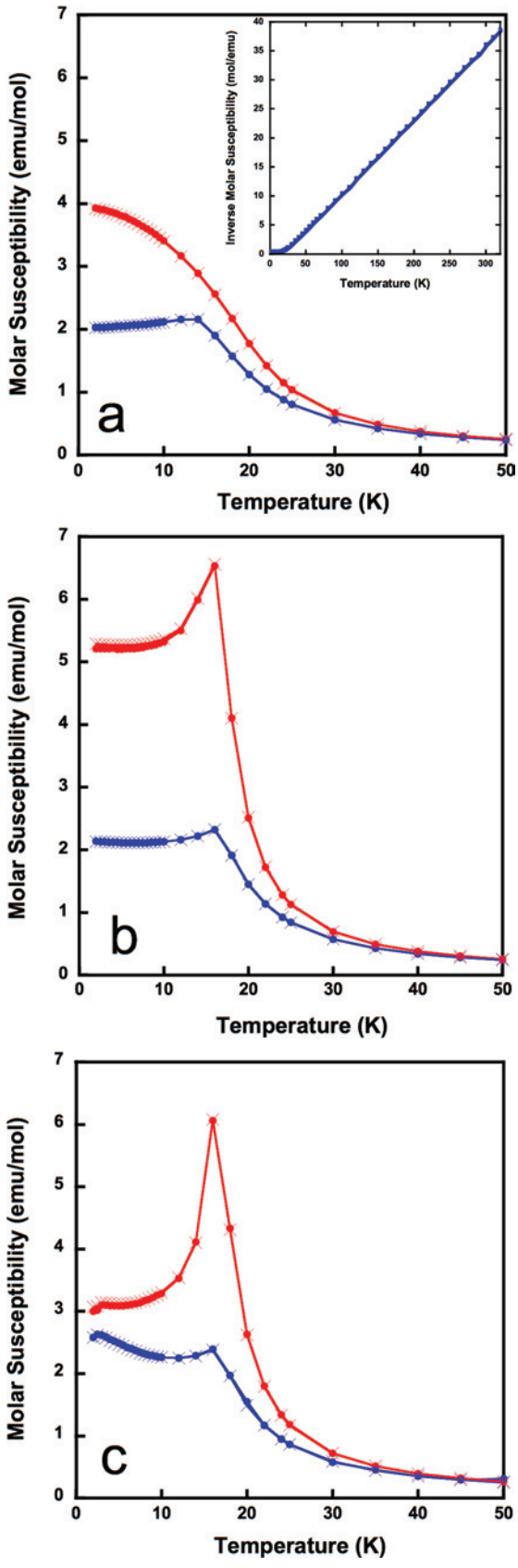


**Figure 3.** Susceptibility versus temperature plots for $EuIn_2As_2$ at (a) 1 T (inset: inverse susceptibility versus temperature), (b) 0.1 T and (c) 0.01 T. Red: *c*-axis is perpendicular to the applied field. Blue: *c*-axis is parallel. Filled circles and X are ZFC and FC data, respectively. ZFC/FC data are coincident.

of the Eu spins. Though both low field data sets indicate antiferromagnetic ordering of the spins in both orientations, for the 1 T measurement with the *c*-axis oriented perpendicular to H, the susceptibility continuously increases upon cooling to the lowest measured temperature, consistent with ferromagnetic rather than antiferromagnetic ordering of the cation spins. Furthermore, upon increasing the field from 0.1 to 1 T in the perpendicular orientation, the ferromagnetic ordering from 45 K > $T$ > 16 K is suppressed.

The collective magnetization versus temperature data indicates both ferro- and antiferromagnetic contributions to the magnetism. A canted magnetic system with both ferromagnetic intralayer and antiferromagnetic interlayer exchange interactions was proposed for the isostructural compound $EuIn_2P_2$,[17] and this model is consistent with the magnetic behavior of $EuIn_2As_2$ reported here. On the basis of structural considerations, one might expect two important Eu···Eu magnetic interactions: strong intralayer and weaker interlayer. For $EuIn_2As_2$, when the *c*-axis is oriented parallel to H (i.e., the cation layer stacking direction is parallel to H), the $\chi$ versus $T$ plots show antiferromagnetic ordering transitions regardless of the applied field, consistent with a model where neighboring layers order ferromagnetically, but possess opposite spins. However, as the field is increased to 1 T in the perpendicular orientation (i.e., the cation layer stacking direction is perpendicular to $H$), the observed susceptibility from 45 K > $T$ > 16 K is reduced, indicating that at higher fields the interlayer Eu cations can interact more strongly, reducing the overall moment due to intralayer ferromagnetic ordering and diminishing the differences between perpendicular and parallel orientations. Furthermore, the continuous increase in the low temperature susceptibility when the *c*-axis is perpendicular to $H$ is consistent with a spin-canted model, where antiparallel interlayer spins have a net component in the *a*-*b* plane that aligns with the field, thus resulting in the observation of weak ferromagnetism (canted antiferromagnetism). Additionally, the coincidence of ZFC and FC data support this model (Supporting Information, Figure S1), in which intralayer spins couple ferromagnetically and interlayer spins couple antiferromagnetically, since the observed triangular arrangement of Eu atoms within individual layers would lead to spin frustration in the case of an antiferromagnetic intralayer exchange interaction. Finally, the Weiss constant is positive in sign at all measured fields, indicating that intralayer ferromagnetic coupling, a necessary condition for interlayer antiferromagnetic coupling, is the dominant exchange interaction.

The magnetization versus field data ($T$ = 5 K, Figure 4), also support the proposed magnetic spin structure with two interacting layers. When the *c*-axis is parallel to the field, the curve rises gradually and linearly, indicating that neighboring layers are antiferromagnetically coupled, and the magnetization begins to saturate at approximately 2 T (7.1(1) $\mu_B$ at 4 T). The measured saturation magnetization in this orientation is slightly greater than is expected for a single $Eu^{2+}$ ($M_{sat}$ = 7.0 $\mu_B$), but is within the standard deviation. Conversely, when the *c*-axis, and consequently the cation layers, are oriented perpendicular to the applied field, the

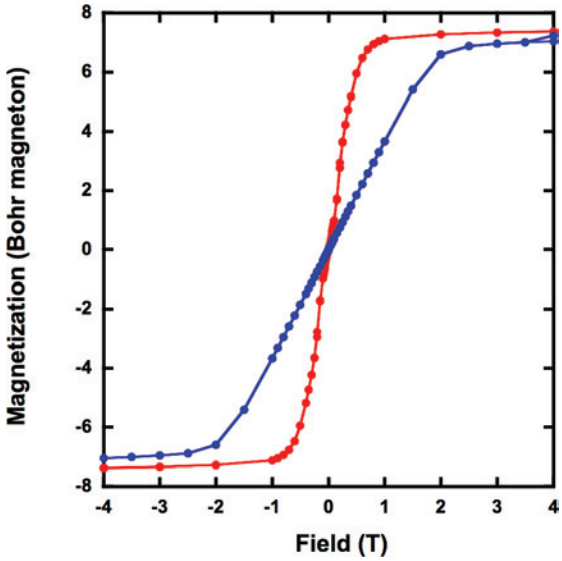


**Figure 4.** Magnetization versus field as a function of crystallographic orientation for $EuIn_2As_2$ at 5 K. Red: *c*-axis is perpendicular to the applied field. Blue: *c*-axis is parallel.

curve rises much more sharply and becomes saturated at lower field (approximately 1 T), and the measured saturation moment (at 4 T) is 7.378(2) $\mu_B$, slightly higher than that expected for a single $Eu^{2+}$. This larger than expected value may be due to crystal shape, an orientation effect, or contributions from the supporting tape in the sample holder. Though saturation is achieved at relatively low field strengths when the *c*-axis is perpendicularly oriented to *H*, indicating soft ferromagnetism, no hysteresis is observed. Instead there is a low field region, from approximately −0.1 to 0.1 T, where the susceptibility rises gradually and linearly with increasing field before increasing more rapidly with small changes in field, which may indicate a spin reorientation (an expanded view of the magnetization versus field data highlighting the behavior in the low field region is shown in Supporting Information, Figure S2), such as a change in canting angle.

The distance between nearest neighbor Eu cations within layers in $EuIn_2As_2$ is 4.207 Å (4.083 Å for $EuIn_2P_2$), and the shortest distance between Eu cations in neighboring Eu layers is 8.945 Å (8.797 Å for $EuIn_2P_2$). Thus, intralayer ferromagnetic coupling rather than interlayer antiferromagnetic coupling should be strongest, as indicated by a positive value for the Weiss constant (17.4 and 24 K, for $EuIn_2As_2$ and $EuIn_2P_2$, respectively). The mechanism of both intralayer and interlayer coupling of the cation spins is likely indirect exchange, occurring via coupling of localized cation moments and delocalized electron spin moments, since at these cation−cation distances communication via direct orbital overlap or through an intervening pnicogen atom (superexchange) is unlikely. Superexchange as a mechanism for spin ordering has been proposed for Eu-containing phases with Eu···Eu distances similar to those involved in the intralayer exchange.[40] However, the distance between oppositely oriented, ferromagnetic layers is certainly too large to couple

(40) Kufnnes, J.; Ku, W.; Pickett, W. E., Los Alamos Laboratory, Preprint Archive, Condensed Matter 2004, arXiv: Condmat/0406229, 1−4.

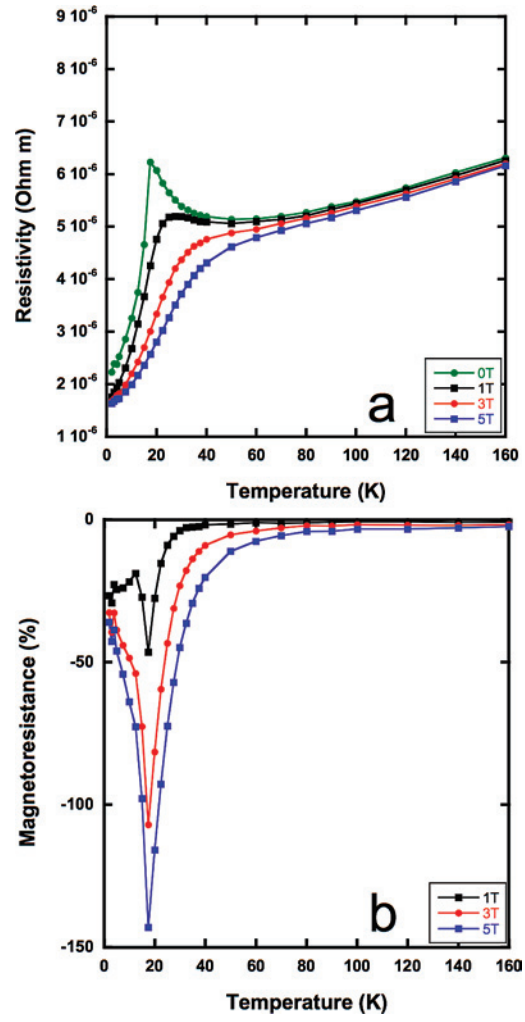


**Figure 5.** (a) Resistivity and (b) magnetoresistance of $EuIn_2As_2$ as a function of temperature under different applied magnetic fields.

the spins via direct or superexchange. Consequently, it is likely that the coupling occurs via indirect exchange, such as Bloembergen−Rowland or RKKY-type coupling, where the local spin moment polarizes delocalized carriers and the polarized carrier wave function overlaps with neighboring local spins to order the local spin moments. As we will discuss in the next section, indirect exchange as the mechanism of spin-ordering is reasonable, since $EuIn_2As_2$ has a resistivity transition associated with a magnetic ordering transition.

**Resistivity and Magnetoresistance.** Standard four probe resistivity measurements were made in zero and higher applied fields on $EuIn_2As_2$ because of the large, negative colossal magnetoresistance (−298% at 24 K, 5 T) observed for $EuIn_2P_2$.[17]

When $EuIn_2As_2$ is cooled from room temperature in the absence of an applied field (Figure 5a), its resistivity decreases with decreasing temperature, consistent with metallic behavior. At 300 K in zero field, the measured resistivities for the previously reported $EuIn_2P_2$ and for the title compound $EuIn_2As_2$ are $2 \times 10^{-5}$ and $7(3) \times 10^{-6}$ Ω m, respectively (See Supporting Information, Figure S3). The resistivity trend is therefore $EuIn_2P_2 > EuIn_2As_2$, consistent with the expected trend toward increased metallicity (de-

creased resistivity) upon descending the periodic table. Over the entire temperature range, both compounds may be classified as metals on the basis of the order of magnitude of their electrical resistivities. However, resistivity values are intermediate between those expected for a semiconductor and a conventional metal such as Cu, and the compounds may therefore be classified as relatively poor metals or semimetals.

For $EuIn_2As_2$, the high temperature data (150−300 K, Supporting Information, Figure S4) indicates that the impact of the magnetic field on the resistivity is negligible, that is, less than 3% magnetoresistive behavior is observed at 150 K. However, despite the high temperature metallic behavior of $EuIn_2As_2$, an increase in resistivity with decreasing temperature is observed in the zero field measurement at temperatures slightly greater than the ordering temperature of 16 K. The increased zero field resistivity in this temperature region (17.5−50 K) can be attributed to increased spin scattering of the carriers by the localized magnetic moments as they begin to spontaneously order over a short-range. Importantly, short-range magnetic ordering of local spins in fluctuating or induced ferromagnetic domains has been reported for other magnetically ordering, magnetoresistive compounds; such spin fluctuations have been linked to both MR and superconducting behavior.[21] The observed zero-field resistivity increase prior to magnetic ordering is characteristic of Kondo-type behavior, where the delocalized carrier effective mass, and thus the electrical resistivity, is changed dependent upon the alignment of the local spins. Recent field dependent optical property measurements in the far IR region on $EuIn_2P_2$ support a Kondo-type transition, coincident with magnetic ordering of the local spins.[18]

Once the local spins are aligned, at or below the magnetic ordering temperature, the carriers experience decreased scatter from the cooperatively aligned local moments, and thus, the zero-field resistivity again decreases with decreasing temperature (2−17.5 K). When a field is applied, the tendency of the magnetic cation spins to order is increased, which results in suppression of the zero field resistivity increase.

Magnetoresistance is not expected for substances having metallic conductivity, and typical metals have magnetoresistance of less than 2%.[41] However, $EuIn_2As_2$ is a metallic compound that has localized magnetic moments in addition to 2-dimensional, conductive layers; consequently, the local spin alignment can affect resistivity in a temperature and field dependent fashion because of magnetic scattering of the electrical carriers by the local moments. For metallic magnets with band structures having valence levels lying near expected metal−insulator transitions, colossal magnetoresistance is frequently observed. For example, we have previously observed colossal magnetoresistance in the $A_{14}MnPn_{11}$ (A = Ca, Sr, Ba, Yb, or Eu; Pn = As, Sb, or Bi) magnetic Zintl phases, where the temperature dependence of the resistivity ($T > T_c$) classifies the arsenides as semiconductors, the antimonides as semimetals, and the bismuthides as metals. On the basis of the classical definition of Zintl phases, which requires every atom to have a closed shell electronic configuration, $EuIn_2As_2$ is expected to be semiconducting with an energy gap between filled and unfilled levels. However, $EuIn_2As_2$ and the isostructural phosphide are metallic phases, as evidenced by the charge transport measurements, and the phases do not encompass a metal−insulator boundary. Despite this, $EuIn_2As_2$ also exhibits colossal magnetoresistance (−143%, 17.5 K, 5 T, Figure 5b), which is most pronounced near the magnetic ordering temperature, although in the present case, maximal MR is observed near an antiferromagnetic ordering transition, rather than near $T_c$, as in the $A_{14}MnPn_{11}$ compounds. However, negative colossal magnetoresistance has been observed for other, semimetallic Eu-containing antiferromagnets, such as the $Eu_xCa_{1-x}B_6$ series, $Eu_{14}MnBi_{11}$, and $EuAs_3$,[9,41,42] and it has been proposed that magnetoresistance results from changes in carrier effective mass and carrier concentration dependent on the local spin alignment. Despite the occasional observation of magnetoresistance in magnetically ordering semimetals, magnetic ordering in combination with metallic conductivity is not a sufficient criterion for MR behavior, and the origin of this property is still unclear. Because of the metallic conductivity observed for these phases, spin exchange via indirect RKKY-type coupling is reasonable, but further theoretical work is necessary to gain further insight. However, one common structural feature of the known magnetoresistant Eu-containing phases is one short and at least one longer M···M distance (M = magnetic cation, e.g., Eu and Mn), which result in multiple exchange interactions, suggesting that magnetic anisotropy may be important in the development of the MR property.

For the $EuIn_2Pn_2$ compounds (Pn = P, As), the zero field resistivity is maximal near the Néel temperature, at $T = 24$ and 17.5 K for $EuIn_2P_2$ and $EuIn_2As_2$, respectively ($T_N$ = 24 and 16 K, respectively). The magnetoresistance is also maximal for both compounds at the temperature corresponding to the zero field resistivity maxima in the largest measured field (5 T). The compounds are negative colossal magnetoresistant materials, with maximal magnetoresistance of −298 and −143% for $EuIn_2P_2$ and $EuIn_2As_2$, respectively. Within the isostructural pair, the maximal magnetoresistance decreases from the phosphide to the arsenide member, which is expected on the basis of the magnetic coupling strength. For the phosphide, which has shorter Eu···Eu distances relative to the arsenide, larger Weiss constants and higher ordering temperatures indicate a more favorable exchange energy (lower energetic barrier to coupling), meaning that the local moments are more tightly coupled in the phosphide. Supportive of this, the dominant ferromagnetic interaction when the *c*-axis is perpendicular to H is seen for $EuIn_2P_2$ at lower field strengths relative to $EuIn_2As_2$. Since communication of the local moment spin alignment likely occurs through the conduction electron wave function, more tightly coupled local spins will have a greater influence on the delocalized carriers, thus leading to greater magnetoresistance.

(41) Chan, J. Y.; Kauzlarich, S. M.; Klavins, P.; Shelton, R. N.; Webb, D. J. *Phys. Rev. B* **1998**, *57*, 57.

(42) Bauhofer, W.; McEwen, K. A. *Phys. Rev. B* **1991**, *43*, 13450.

## Conclusions

In an effort to develop structure/property and composition/property relationships in magnetic Zintl phases exhibiting colossal magnetoresistance, $EuIn_2As_2$ was synthesized as a heavier pnicogen analogue of $EuIn_2P_2$. The two compounds are isostructural, and have a new structure type. They have similar, anisotropic magnetic behaviors, which result from intralayer and interlayer magnetic exchange interactions in the layered, hexagonal structure type. In one crystallographic orientation, antiferromagnetic transitions are observed for the arsenide and the phosphide respectively, at 16 and 24 K; both compounds additionally exhibit features of ferromagnetic ordering in the opposite orientation, although the extent of ferromagnetic ordering is affected by the differing Eu···Eu distances in $EuIn_2P_2$ versus $EuIn_2As_2$, and these features arise in applied fields of differing magnitudes. The higher ordering temperature of the phosphide indicates a greater magnetic coupling strength in this compound compared to the arsenide, which is expected based on the shorter cation−cation distances in the compound containing the smaller pnicogen. The temperature dependent resistivity measurements indicated that both compounds are metallic, with sharp increases in resistivity at temperatures slightly greater than their magnetic ordering temperatures. The resistivity increase is suppressed with increasing field, and both compounds exhibit negative colossal magnetoresistance, which is likely mediated indirectly by the carrier spin alignment.

Despite the fact that both $EuIn_2P_2$ and $EuIn_2As_2$ are metallic and do not span a metal−insulator border, the trends of decreased ordering temperature, decreased resistivity and decreased CMR with heavier pnicogen analogues observed for the $A_{14}MnPn_{11}$ series also apply to the $AM_2X_2$ pair reported here. Consequently, one might predict loss of the CMR behavior in the heavier pnicogen analogues $EuIn_2Sb_2$ and $EuIn_2Bi_2$, which have yet to be synthesized, assuming that the structure type is retained.

**Acknowledgment.** This work was supported by the National Science Foundation (Grants DMR-0600742 and DMR-0645461). A.M.G. acknowledges a Career Award at the Scientific Interface from the Burroughs Wellcome Fund (Award 1007294) for support.

**Supporting Information Available:** Additional crystallographic data for $EuIn_2As_2$ in CIF format, susceptibility (2−320 K) as a function of temperature, an expanded view (−1 to 1 T) of magnetization versus field, and resistivity and magnetoresistance (2−300 K) as a function of temperature and field. This material is available free of charge via the Internet at http://pubs.acs.org.

IC801290U